Layered double hydroxide and sulindac coiled and scrolled nanoassemblies for storage and drug release

Michele A. Rocha,[a] Philippe A. D. Petersen,[b] Erico Teixeira-Neto,[c] Helena M. Petrilli,[b] Fabrice Leroux,[d] Christine Taviot-Gueho,[d] and Vera R. L. Constantino*[a]

[a]Departamento de Química Fundamental, Instituto de Química, Universidade de São Paulo, C. P. 26077, CEP 05513-970, São Paulo – SP, Brazil.

[b]Instituto de Física, Universidade de São Paulo, C. P. 66318, CEP 05315-970, São Paulo - SP, Brazil.

[c] Laboratório Nacional de Nanotecnologia, CNPEM, C. P. 6192, CEP 13083-970, Campinas-SP, Brazil.

[d] Université Clermont Auvergne, Université Blaise Pascal, Institut de Chimie de Clermont-Ferrand, BP 10448, F-63000 Clermont-Ferrand, France, CNRS, UMR 6296, ICCF, F-63178 Aubiere, France.

Electronic supplementary information (ESI)

A brief description of the models used in the present work is given ahead.

Zero order model:

$$1 - \frac{M_t}{M_0} = M_0 - \mathrm{k}_0 t \quad (1)$$

where M_t is the amount of drug released at time t, M_0 is the initial amount of the drug in the pharmaceutical formulation and k_0 is the zero order constant. A graphic of the non-delivered fraction of the drug *versus* time is linear and the intercept with the y-axis is M_o (M_o = 1).

First order model:

$$\ln(M_0 - M_t) = \ln \mathrm{M}_0 - \mathrm{k}\, t \quad (2)$$

where M_t is the amount of drug released at time t, M_0 is the initial amount of the drug in the carrier. A graphic of Naperian logarithm the non-delivered fraction of the drug *versus* time is linear and the intercept with the y-axis is $\ln M_o$ (M_o = 1). According to this model, the release is proportional to que amount of drug kept on the carrier.

Korsmeyer –Peppas and Higuchi models:

$$\frac{M_t}{M_0} = \mathrm{k}t^n \; or \; \log\frac{M_t}{M_0} = \log k + n\log t \tag{3}$$

where M_t is the drug mass release at time t, M_0 is drug mass at $t = 0$, M_t/M_0 is a fraction of drug released at time t, k is the release rate constant and n is the release exponent (which give information about the drug transport mechanism).[1] If $n = 1$, the mechanism is of zero-order and the release does not depend neither on the drug amount in the carrier nor on the systems geometry (thin films, spheres, cylinders, etc.). On the other hand, if $n = 0.5$ the mechanism is described by the Higuchi model that presumes a Fickian diffusion as the rate limiting step. When $0.5 < n < 1$, an anomalous (non-Fickian) transport is assumed. The mathematical models described are useable only for the range up to 60% ($M_t/M_0 = 0.60$) of the drug release and from thin slabs or sheets (one-dimensional diffusion).[2]

Hixson-Crowell model:

$$\left(1 - \frac{M_t}{M_0}\right)^{\frac{1}{3}} = 1 - K_\beta t \tag{4}$$

where M_t is the drug mass release at time t, M_0 is drug mass at $t = 0$, and K_β is the release constant. Then, a graphic of the cubic root of undissolved fraction of drug *versus* time should be linear. This model assumes a spherical drug particle and a dissolution occurring with no fragmentation into smaller particles but with modifications of the surface area and particle diameter with time.[3]

Bhaskar model:

$$-ln\left(1 - \frac{M_t}{M_0}\right) = ln\left(\frac{M_0}{M_0 - M_t}\right) = 1.59\left(\frac{6}{d_p}\right)^{1.3}(Dt)^{0.65} \tag{5}$$

where particle diffusion control can be tested by simply testing for linearity between $\ln(M_0/(M_0\text{-}M_t)$ and $t^{0.65}$.[4] This model has been used to drug delivery from resinates (ionic

drugs immobilized into organic ion exchangers) and assumes a pore/particle diffusion resistance controlled mechanism. M_t is the drug content release at time *t*, M_0 is drug content of resinate at $t = 0$, d_p is the resin particle diameter and D is the release constant.

Parabolic diffusion model:

This model is used in the case of diffusion-controlled phenomena. It is based on a radial diffusion in a cylinder assuming a constant and uniform concentration at the beginning of the diffusing species on the cylindrical surface and throughout the cylinder.[5] Species diffusion through the upper and lower faces of the cylinder is supposed insignificant; the equation can be expressed as:

$$\left(\frac{M_t}{M_0}\right) = \frac{4}{\pi^{0.5}}\left(\frac{Dt}{r^2}\right)^{0.5} - \frac{Dt}{r^2} \qquad (6)$$

where M_t is the quantity of diffusing species that has left the cylinder at time *t*, M_0 is the corresponding quantity at equilibrium, *r* is the radius of cylinder and *D* is the diffusion coefficient. A graph of $(M_t/M_0)/t$ *vs* $1/t^{0.5}$ is linear assuming a radial diffusion of species in solids with exchange sites difficult to access as for soils constituents. According to this model, the reaction rate is controlled by intraparticle diffusion; it has been used for example to described metallic ion adsorption and desorption on the soil constituents and feldspar.[6,7]

RESULTS AND DISCUSSION

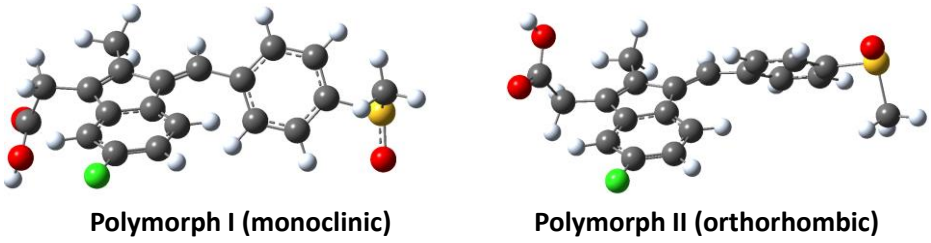

Fig. S1 Polymorphs of sulindac obtained by DFT calculation according to structures reported by Grzesiak *et al.*[8] (polymorph I, CCDC Nº. 625435) and Koo *et al.*[9] (polymorph II, CSD entry "Dohrex").

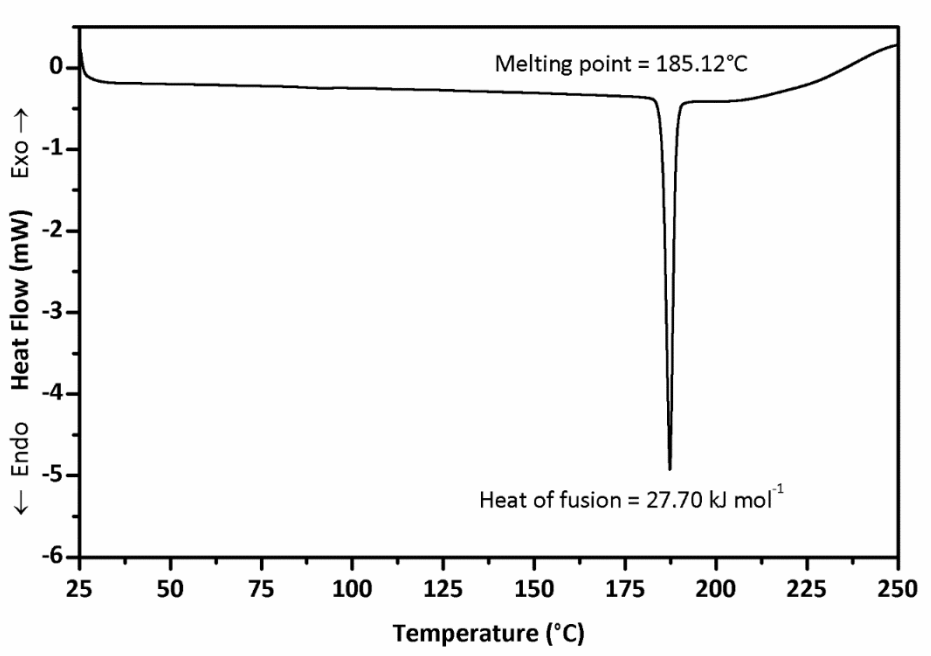

Fig. S2 DSC curve of sulindac (protonated form, commercial product).

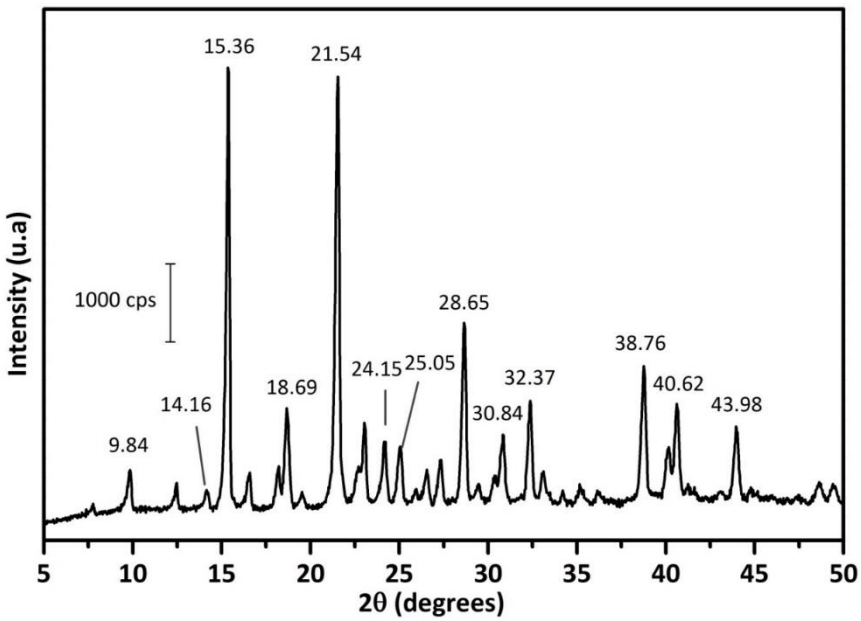

Fig. S3 XRD pattern of sulindac (protonated form, commercial product).

Table S1. X-ray diffraction data (2θ values for CuKα) of sulindac (protonated form, commercial product).

Sulindac 2θ / º	Literature [8] 2θ / º
9.8	9.6
12.5	12.3
14.2	14.0
15.4	15.1
16.6	16.4
18.2	18.5
18.7	19.4
21.5	21.4
23.0	22.5
24.2	24.0
25.1	24.9
26.6	26.3
27.4	27.1
28.6	28.4
29.5	29.2
30.4	30.2
30.8	30.5
32.4	32.1
33.1	33.0
34.2	34.3
35.2	35.0
36.2	36.1
38.8	38.5
40.2	39.9
40.6	40.4
	41.0
43.9	43.8
	44.6
48.6	48.5
49.4	49.3

Table S2. Interplanar distances d_{00l} and 2θ (CuKα) values deduced from XRD data of LDH-Sul samples prepared at room temperature. The indexation of the peaks is based on the R-3m space group.

Mg_2Al-Sul RT		Zn_2Al-Sul RT		
2θ	d (nm)	2θ	d (nm)	hkl
3.80	2.32	3.65	2.42	(003)
8.16	1.08	7.24	1.22	(006)
12.1	0.73	12.3	0.72	(009)
		16.0	0.55	(0012)
		19.7	0.45	(0015)
21.20	0.42	23.3	0.38	(0018)
				(0021)
35.0	0.26	34.1	0.26	(012)
61.3	0.15	60.8	0.15	(110)

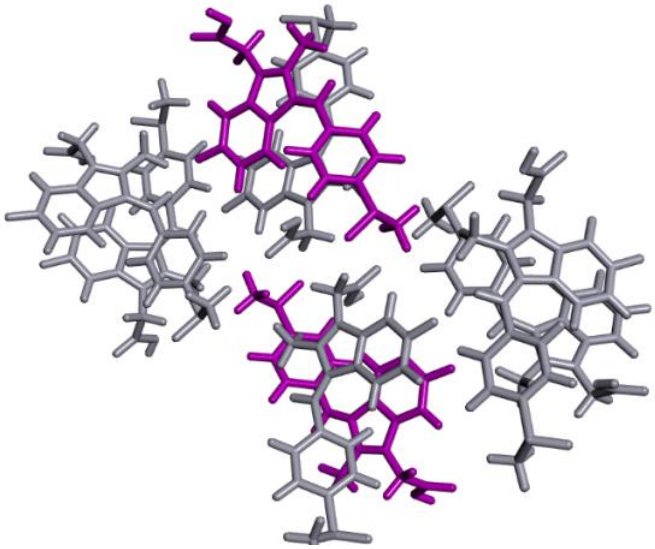

Fig. S4 Part of crystal structure of sulindac (polymorph II)[9] Molecules highlight in pink have an arrangement similar to that one observed for sulindac intercalated between LDH layers in Zn_2Al-Sul 55 sample.

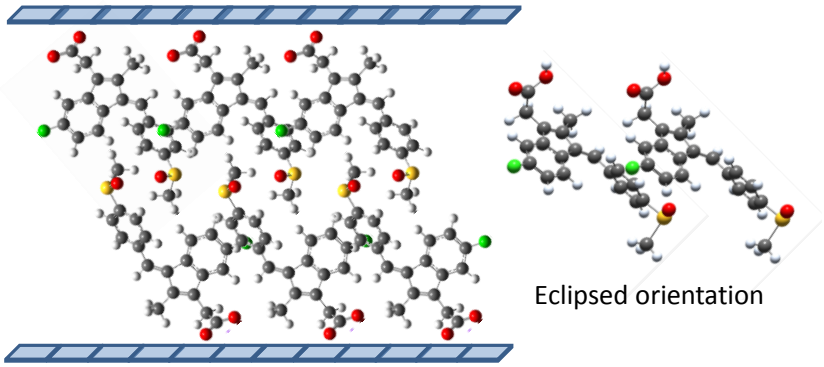

Fig. S5 Eclipsed arrangement of sulindac ions in the interlayer space of M_2Al-LDH materials.

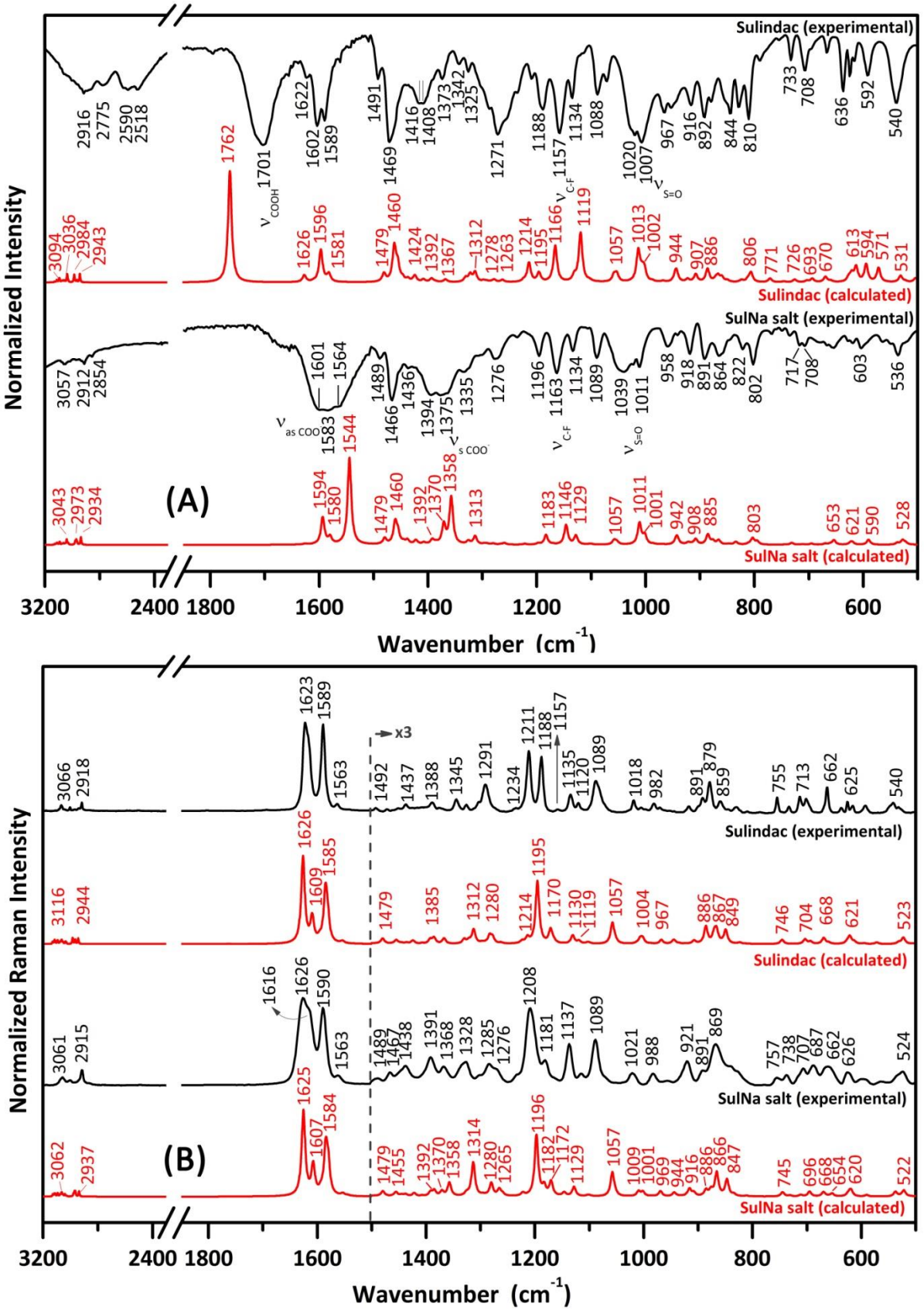

Fig. S6 Experimental and calculated (A) IR and (B) Raman spectra of protonated sulindac and sodium sulindac.

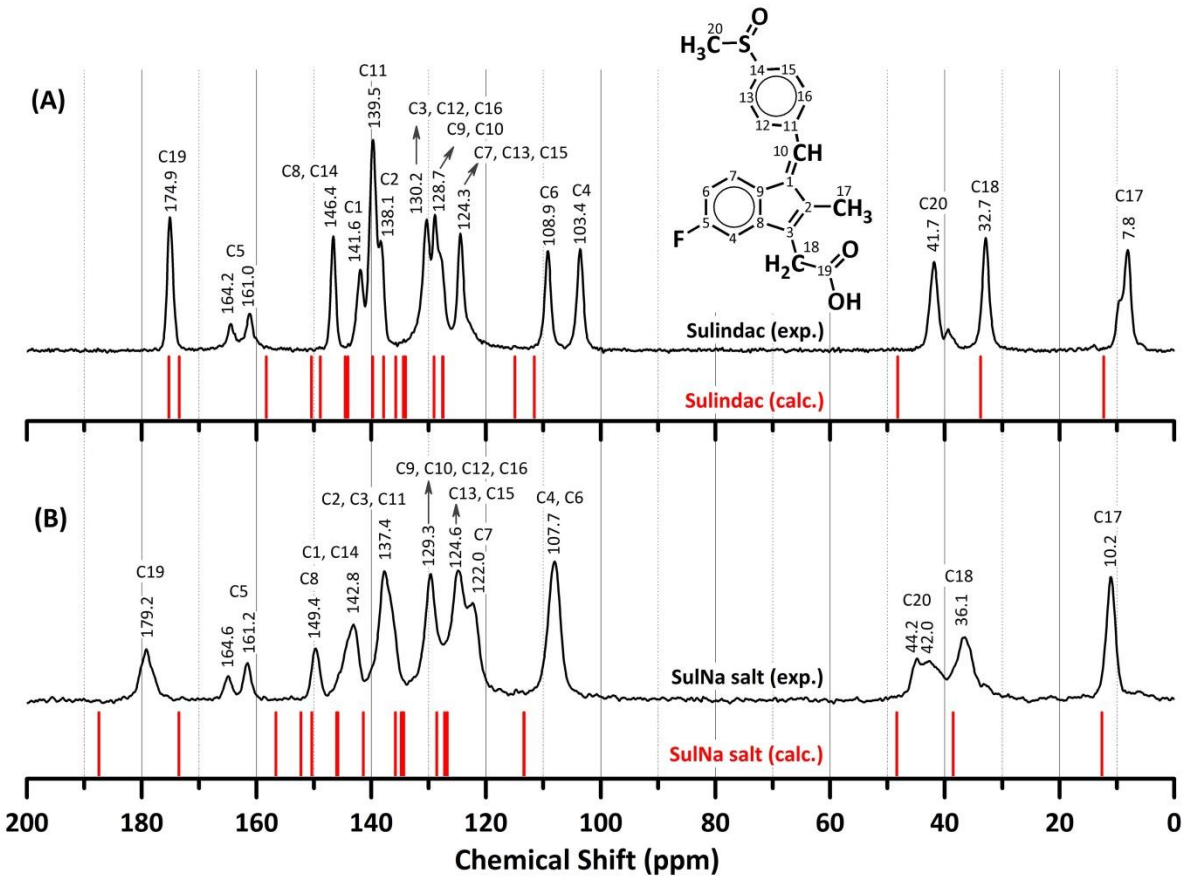

Fig. S7 Solid state ^{13}C-NMR spectra of (A) sulindac and (B) sodium sulindac.

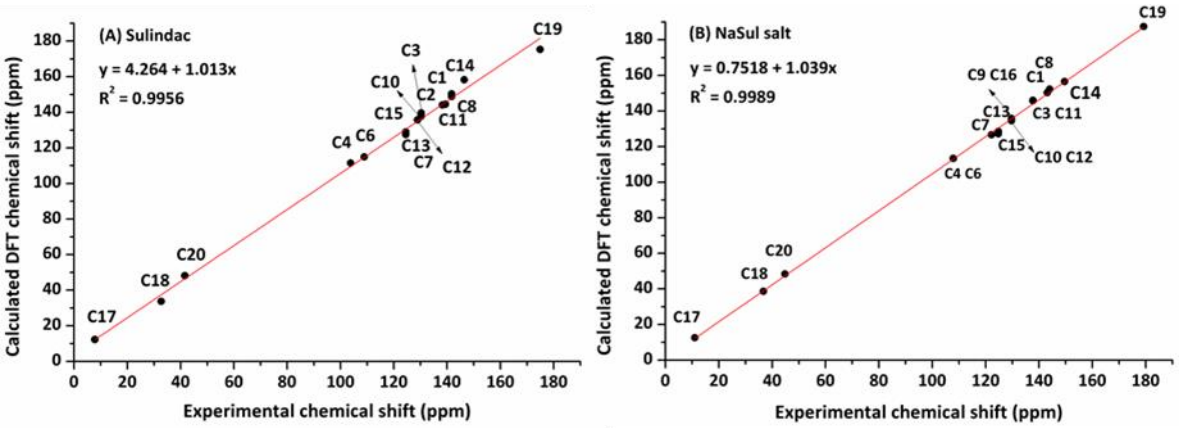

Fig. S8 Correlation between experimental and calculated (DFT method) ^{13}C chemical shifts. Atom C5 was not plotted.

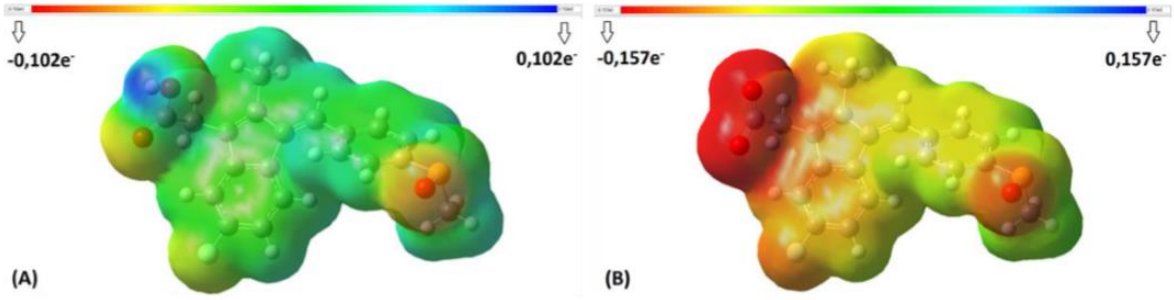

Fig. S9 Map of charge density of sulindac (A) and its deprotonated form (B) calculated by DFT method.

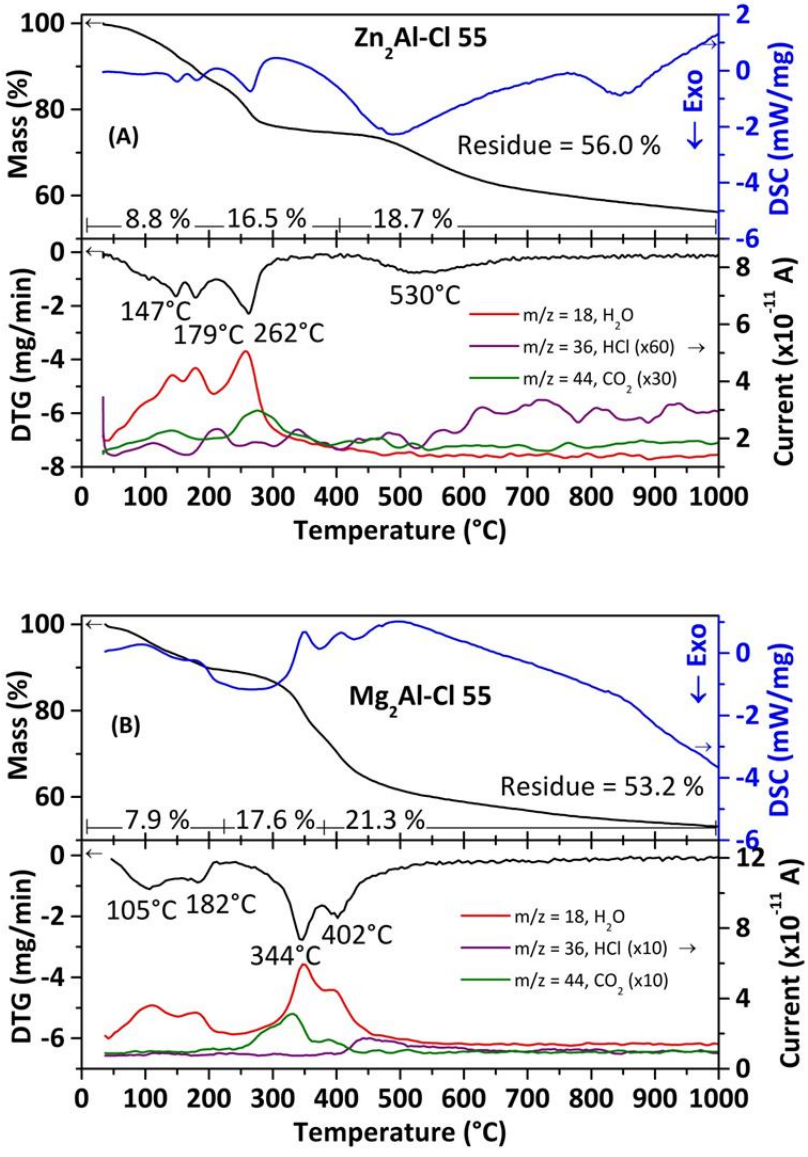

Fig. S10 TG-DTG-MS curves of (A) Mg_2Al-Cl 55 and (B) Zn_2Al-Cl 55 samples.

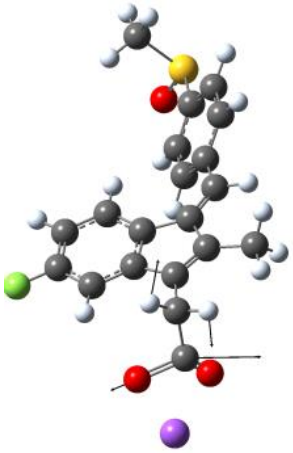 **1558 cm^{-1}** $\nu_{as}COO^{-} + \delta_{ass}(3\text{-}CH_2)$	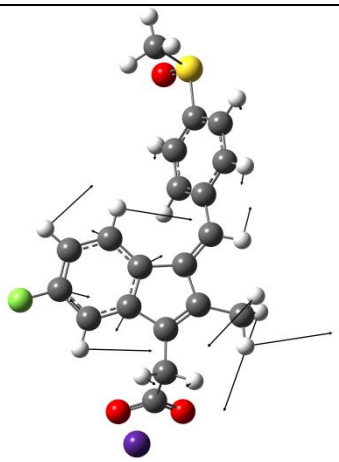 **1466 cm^{-1}** $\delta(2\text{–}CH_3) + \nu(C{=}C) + \delta_{ip}(CH)$ indene ring	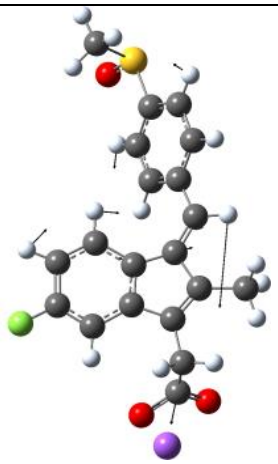 **1380 cm^{-1}** $\nu_s(COO^{-}) + \nu(C\text{-}COO^{-}) + \delta_{ip}(C10\text{-}H)$
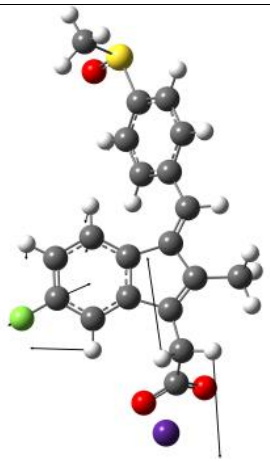 **1196 cm^{-1}** $\nu(C\text{-}F) + \delta_{ass}(3\text{-}CH_2) + \delta_{ip}(CH)$ indene ring	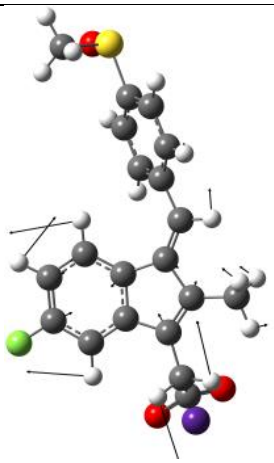 **1163 cm^{-1}** $\nu(C\text{-}F) + \delta_{ass}(3\text{-}CH_2) + \delta(2\text{-}CH_3) + \delta_{ip}(CH)$ indene	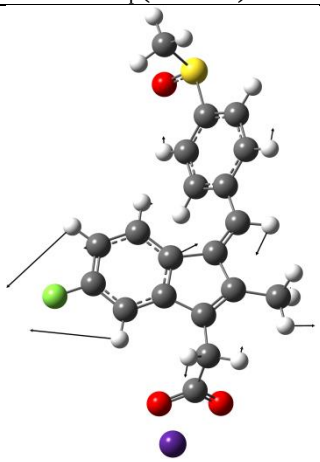 **1135 cm^{-1}** $\delta_{ip}(CH)$ indene + $\delta(2\text{–}CH_3)$
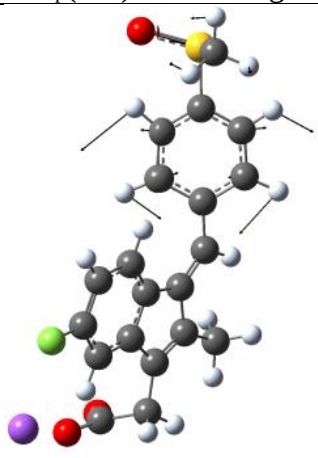 **1045 cm^{-1}** $\nu(S{=}O) + \delta_{ip}(CH)$ phenyl + δCH_3 methysulfinyl	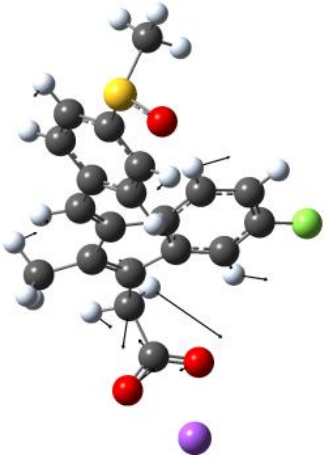 **918 cm^{-1}** $\delta(3\text{–}CH_2) + \delta(COO^{-})$	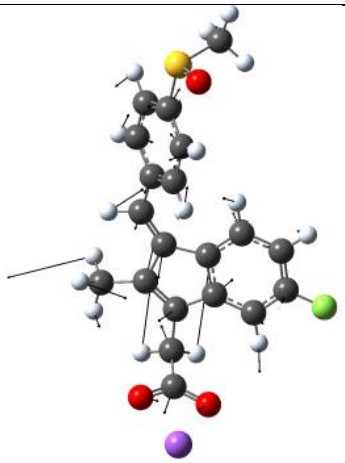 **669 cm^{-1}** $\delta(COO^{-}) + \delta(2\text{-}CH_3) + \delta(3\text{–}CH_2) + \delta_{oop}(C10\text{-}H)$

Fig. S11 Some vibrational modes obtained by DFT calculations.

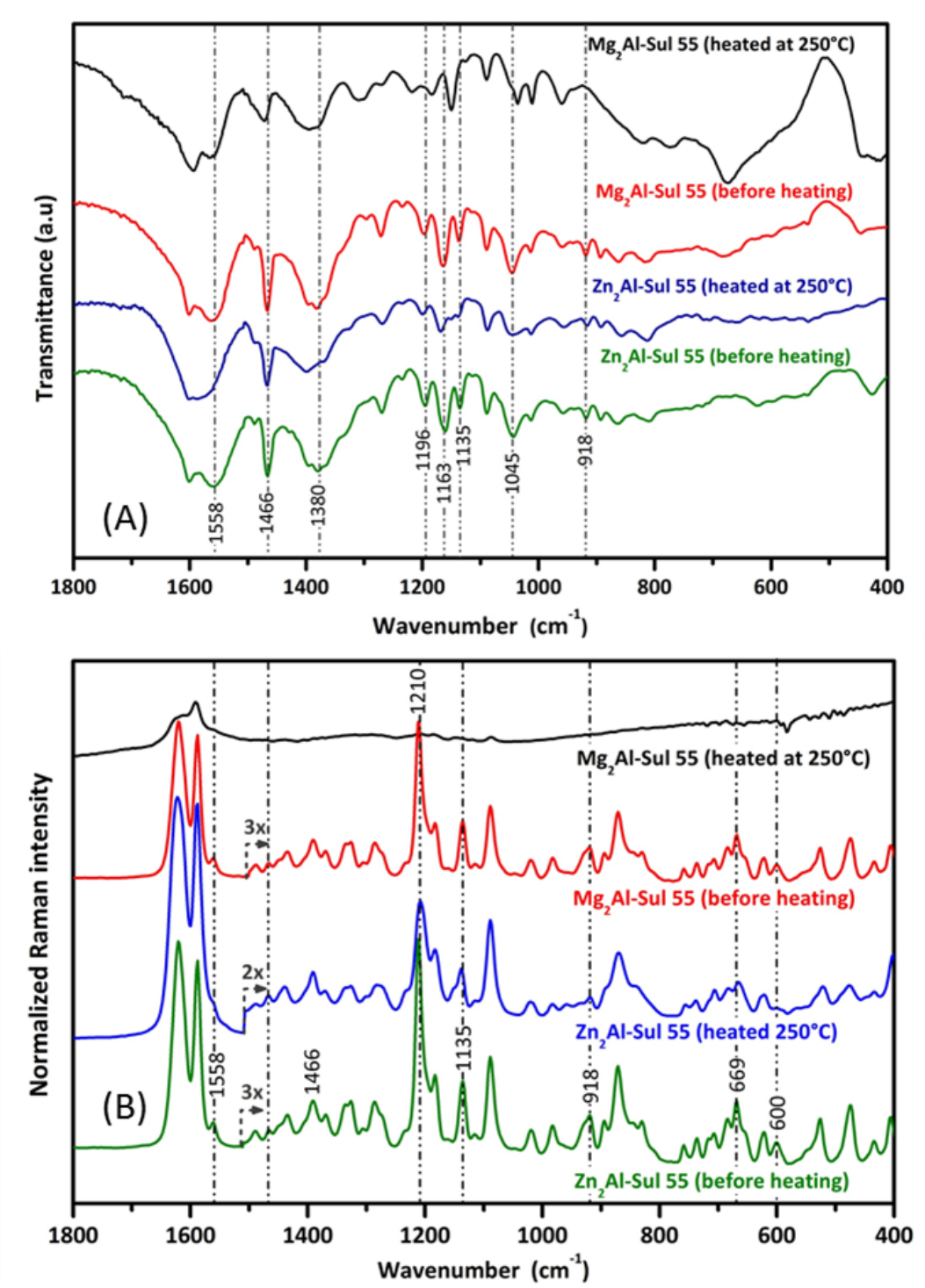

Fig. S12 FTIR (A) and FT-Raman (B) spectra of Mg_2Al-Sul 55 and Zn_2Al-Sul 55 samples before and after heating process at 250ºC in air.

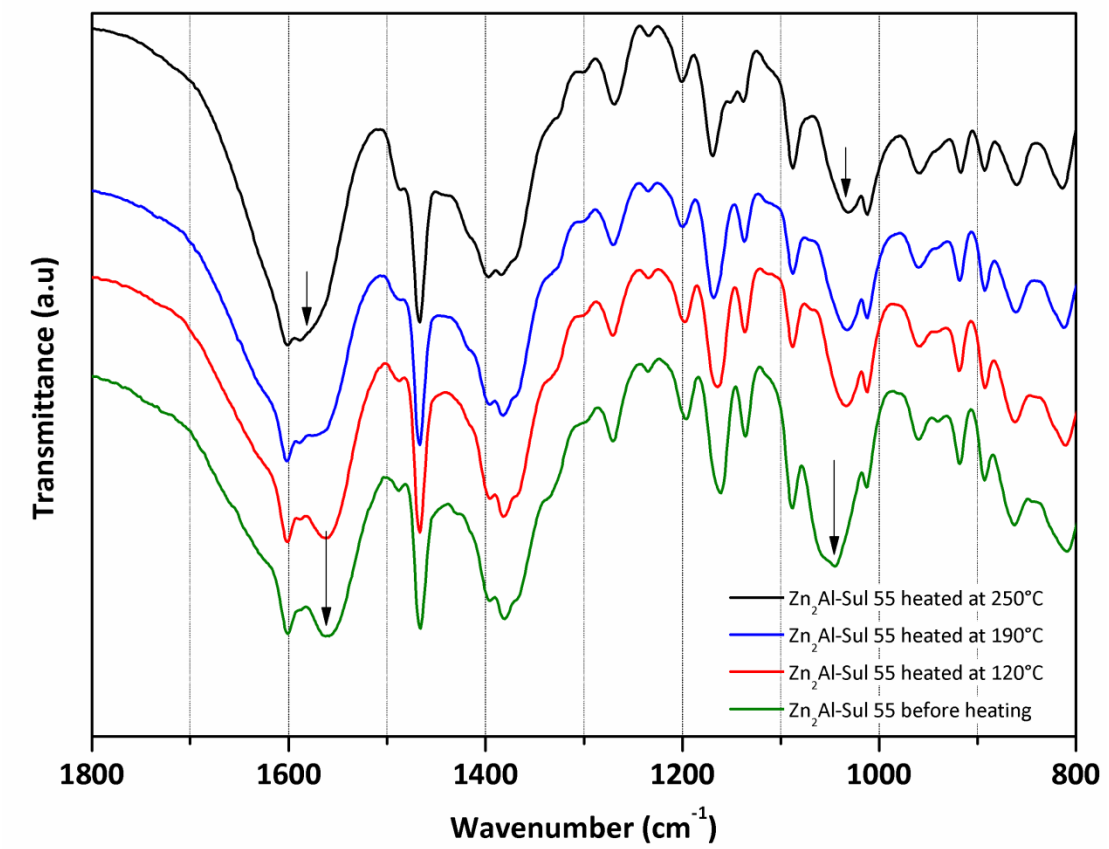

Fig. S13 FTIR spectra of Zn_2Al-Sul 55 sample before and after heating processes at 120ºC (dehydration), 190ºC (dehydroxylation) and 240ºC in air. Mainly modifications are indicated with arrows.

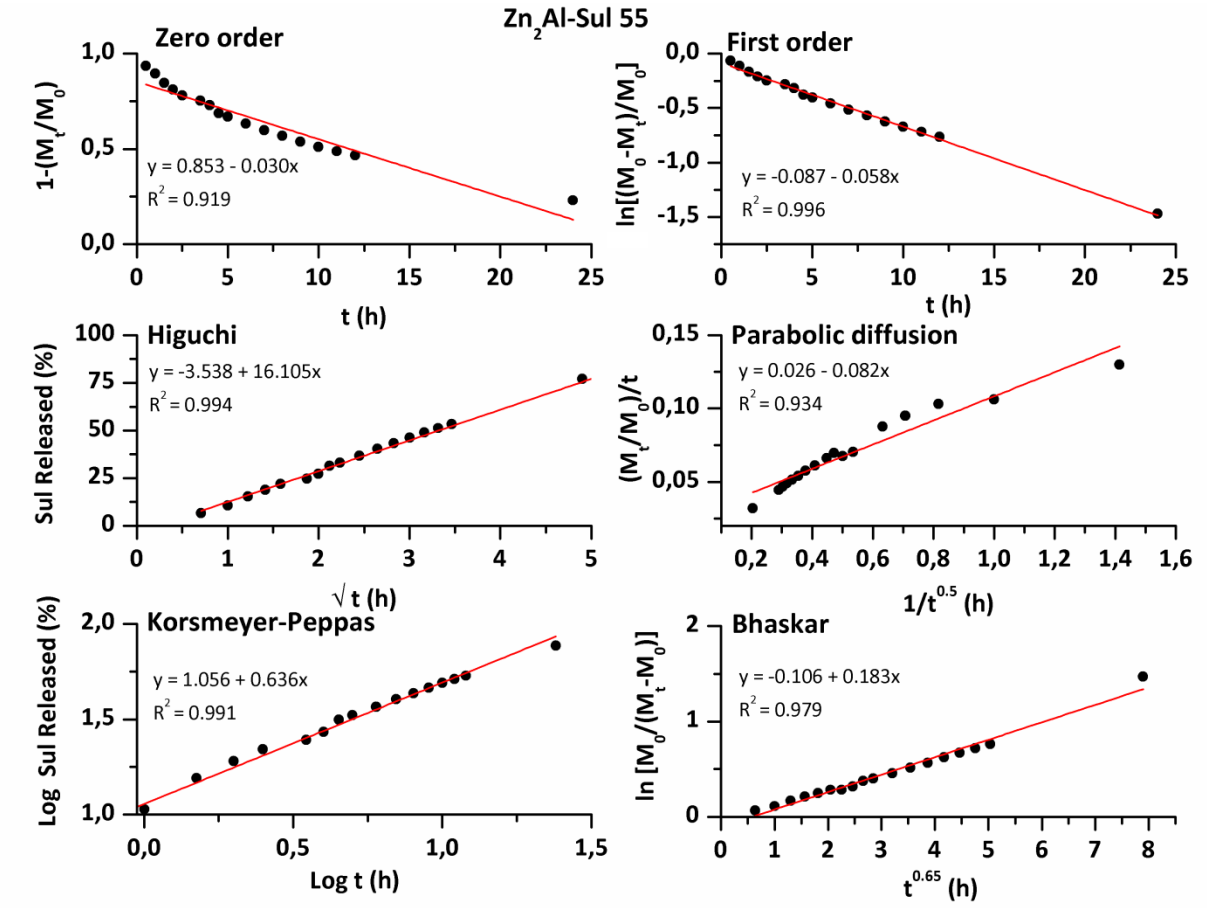

Fig. S14 Kinetic Models applied to Zn_2Al-Sul 55 sample considering 24 h of release.

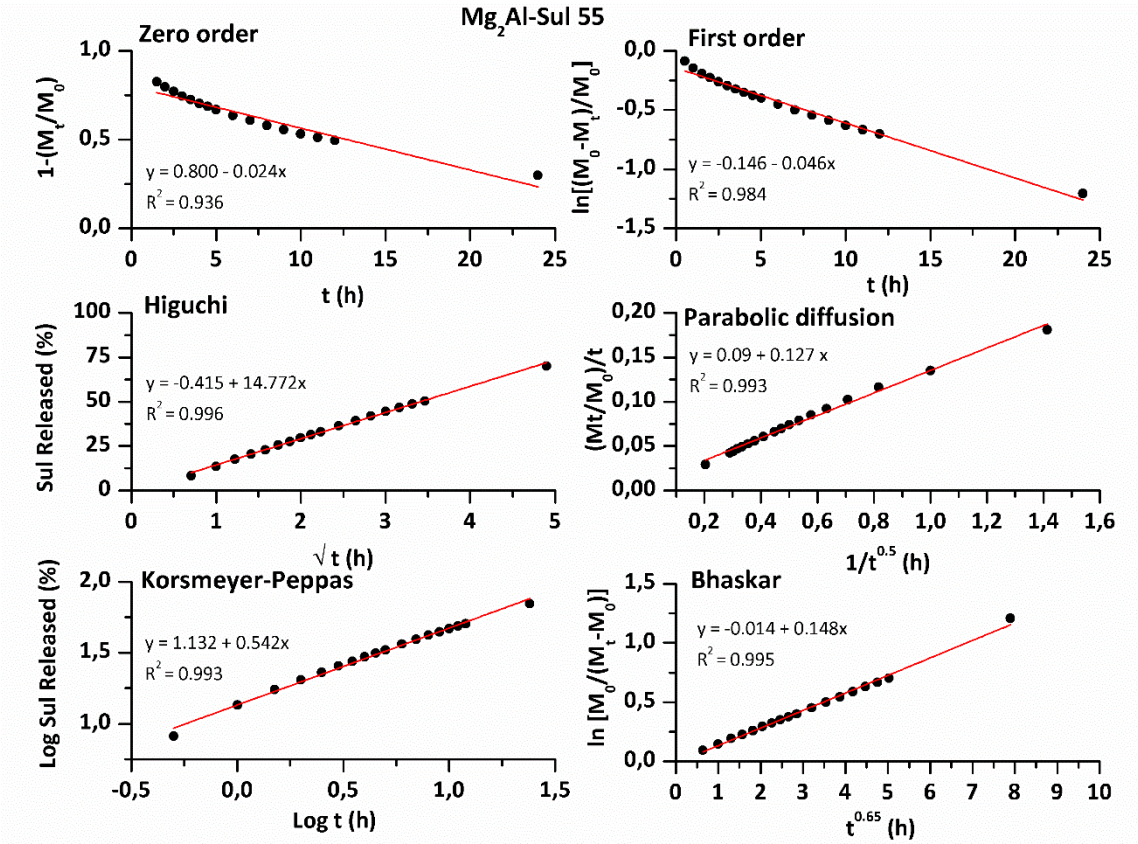

Fig. S15 Kinetic Models applied to Mg_2Al-Sul 55 sample considering 24 h of release.

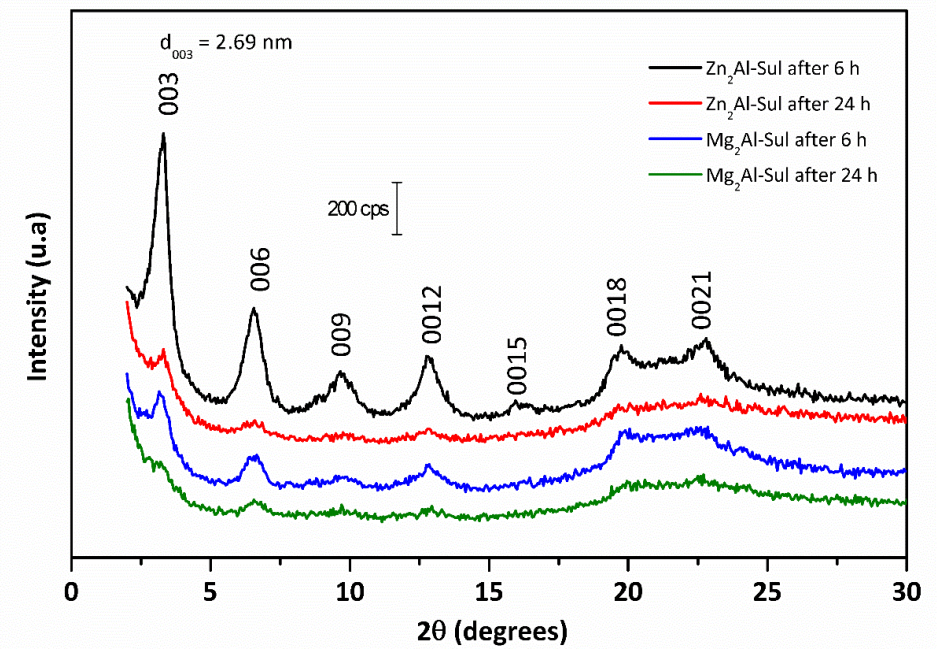

Fig. S16 XRD patterns of M^{II}_2Al-Sul 55 tablets after 6 and 24 h in buffer solution (drug delivery experiment).

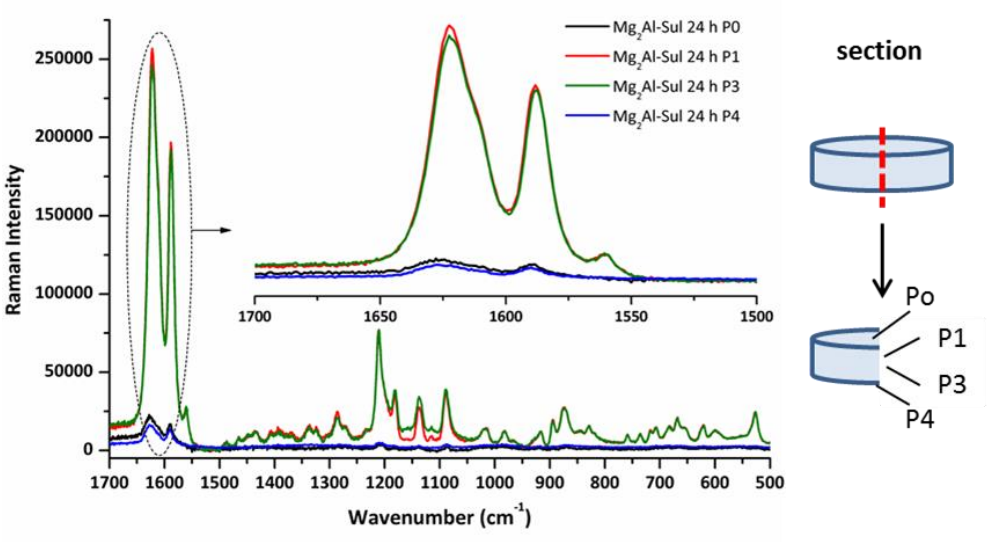

Fig. S17 Raman spectra of Mg_2Al-Sul 55 tablet after 24 h in buffer solution (drug delivery experiment). Laser beam was directed to points P indicated in the right figure (P1 and P4 are regions in the external surface while P1 and P3 are internal regions of the tablet).

References

(1) Ritger, P. L.; Peppas, N. A. *J. Controlled Release* 1987**, 5**, 23-36.
(2) Serra, L.; Doménech, J.; Peppas, N. A. *Biomaterials* 2006**, 27**, 5440-5451.
(3) Siepmann, J.; Siepmann, F. *Int. J. Pharm.* 2013**, 453**, 12-24.
(4) Bhaskar, R.; Murthy, R. S. R.; Miglani, B. D.; Viswanathan, K. *Int. J. Pharm.* 1986**, 28**, 59-66.
(5) Sparks, D. L., Kinetics and Mechanisms of Chemical Reactions at the Soil Mineral-Water Interface In *Soil Physical Chemistry*, 2 ed.; Sparks, D. L., Ed. CRC Press: Boca Raton, FL, 1999; p 432.
(6) Jardine, P. M.; Sparks, D. L. *Soil Sci. Soc. Am. J.* 1984**, 48**, 39-45.
(7) Chute, J. H.; Quirk, J. P. *Nature* 1967**, 213,** 1156-1157.
(8) Grzesiak, A. L.; Matzger, A. J. *J. Pharm. Sci.* 2007**, 96,** 2978-2986.
(9) Koo, C. H.; Kim, S. H.; Shin, W. *Bull. Korean Chem. Soc.* 1985**, 6**, 222-224.